Chinese Chemical Letters 35 (2024) 109336

Contents lists available at ScienceDirect

Chinese Chemical Letters

journal homepage: www.elsevier.com/locate/cclet

Synthesis of carbon quantum dots decorating Bi_2MoO_6 microspherical heterostructure and its efficient photocatalytic degradation of antibiotic norfloxacin

Meijuan Chen[a,*], Liyun Zhao[a], Xianjin Shi[b], Wei Wang[b], Yu Huang[b], Lijuan Fu[a], Lijun Ma[a]

[a] School of Human Settlements and Civil Engineering, Xi'an Jiaotong University, Xi'an 710049, China
[b] Key Lab of Aerosol Chemistry and Physics, State Key Laboratory of Loess and Quaternary Geology (SKLLQG), Institute of Earth Environment, Chinese Academy of Sciences, Xi'an 710061, China

ARTICLE INFO

Article history:
Received 31 August 2023
Revised 13 November 2023
Accepted 22 November 2023
Available online 30 November 2023

Keywords:
Bi_2MoO_6
CQDs
Heterojunction
Norfloxacin
Photocatalysis

ABSTRACT

In this study, three-dimensional microspherical CQDs/Bi_2MoO_6 heterostructures were synthesized using a simple alcohol-thermal method. It was found that the CQDs/Bi_2MoO_6 had a large specific surface area of 56.0 m^2/g, and the introduction of CQDs extended the light absorption spectrum from 480 nm to 496 nm. When utilizing the synthesized CQDs/Bi_2MoO_6 composite for photocatalytic degradation of antibiotic norfloxacin in a water environment, complete decay of norfloxacin and effective removal of total organic carbon (TOC) were achieved within 30 min. Through the optimization of material synthesis and experimental conditions, the optimal CQDs loading amount was determined as 200 μL, the optimal CQDs/Bi_2MoO_6 dosage was 0.8 g/L. Moreover, the CQDs/Bi_2MoO_6 worked well under a wide pH range of 4.4–10.8. The coexistence of HCO_3^- enhanced the norfloxacin decay, while the presence of Cl^-, NO_3^-, and SO_4^{2-} slightly retarded it. The synthesized CQDs/Bi_2MoO_6 had the great potential in removing and mineralizing norfloxacin in real aquatic environments.

Recently, antibiotic contamination has attracted a lot of attention [1]. As one of them, norfloxacin is widely used worldwide as a therapeutic drug and growth promoter due to its excellent properties of low price and stable efficacy, but its massive utilization brings a lot of environmental problems [2]. Moreover, the inefficient operation of conventional wastewater treatment plants in eliminating norfloxacin results in the discharge of norfloxacin into various water sources and causes water pollution [1]. Relevant investigations showed that 960 ng/L and 862 ng/L of norfloxacin were detected in a sewage treatment plant in Finland and Beijing (China), respectively, 2366 ng/L of norfloxacin was detected in sewage in Spain, 2200 ng/L in surface water in Kenya, 1070 ng/L in sewage in Hong Kong, China, and 989 ng/L in rivers in Shanghai, China [1,3]. The input of norfloxacin in the aquatic environment has a negative impact on aquatic organisms, resulting in high ecological and health risks [4]. In an attempt to address concerns about norfloxacin contamination, various technologies have been developed, including adsorption, biodegradation, and photocatalysis [5–7]. Among them, photocatalysis is of great interest owing to inexpensive and stable and is now widely used in water treatment research [8]. The key to the photocatalytic removal of norfloxacin in water is the development of suitable photocatalysts that can absorb natural light to achieve efficient mineralization of norfloxacin in complex environments.

Many recent studies have been devoted to the development of novel antibiotic-degrading materials, but they all have suffered from some limitations, such as the OCN-$MnFe_2O_4$ photocatalyst synthesized by Zeng *et al.* [9] which could only achieve 42.7% ciprofloxacin degradation efficiency at 1 h; MIL-88A(Fe)/cotton fibers (MC) photocatalyst synthesized by Wang *et al.* [10] which could only achieve about 30% tetracycline degradation efficiency at 8 min and which must be accompanied by the addition of the oxidant peroxynitrite to achieve a better degradation efficiency; The Co_3O_4 NPs@N-PC catalyst synthesized by Mohtasham *et al.* [11] also required the addition of oxidant peroxymonosulfate to achieve better degradation efficiency for sulfamethoxazole; The g-C_3N_4/$Ni_{0.5}Zn_{0.5}Fe_2O_4$ catalyst prepared by Dhiman *et al.* [12] was only able to achieve a better antibiotic removal efficiency when the reaction was up to 60 min long. In view of this situation, the most basic Aurivillius oxide, Bi_2MoO_6 displays promising photocatalytic performance towards the breakdown over organic contaminants [13]. Nevertheless, the photocatalytic performance of pure

* Corresponding author.
E-mail address: chenmeijuan@xjtu.edu.cn (M. Chen).

https://doi.org/10.1016/j.cclet.2023.109336
1001-8417/

Bi_2MoO_6 is restricted due to its underutilization of visible light (Bi_2MoO_6 band gap of 2.60–2.90 eV) and the fast recombination of photogenerated electrons and holes [13]. Several publications have reported that the Bi_2MoO_6-based photocatalysts, including those combined with different semiconductors to fabricate composites, such as Bi_2MoO_6/MoO_3 [14], Bi_2MoO_6/WO_3 [15], and Bi_2MoO_6/ZnO [16], showed superior photocatalyst performance because of its fast electron-hole separation. But they still suffered from the limitation of the insufficient visible light response.

Carbon quantum dots (CQDs) has attracted a great deal of interest due to their high visible light absorption intensity, photostability, biocompatibility, and low cytotoxicity [17]. Recently, the composites by coupling CQDs with Bi_2MoO_6 have been proposed as a promising approach to enhance electron-hole separation [18]. For example, Di *et al.* [19] prepared CQDs/Bi_2MoO_6 composites and found that it had 5 times higher photocatalytic activity of pure Bi_2MoO_6. The degradation efficiency on ciprofloxacin reached 88% within 120 min. In the CQDs/Bi_2MoO_6 synthesized by Sun *et al.* [20], although the introduction of CQDs increased the light absorption intensity, it showed ignorable effect on the extending of absorption edge because all the CQDs/Bi_2MoO_6 samples showed the same absorption edge of 479 nm. Therefore, while modifying Bi_2MoO_6 with CQDs to improve photoelectron-hole charge separation, it is also necessary to further improve the visible light absorption performance. Furthermore, the size of the catalyst surface area largely determines the adsorption and conversion efficiency of pollutants by catalysts [19]. However, the reported synthesized CQDs/Bi_2MoO_6 catalyst have relatively small specific surface areas. Considering the relatively low specific surface area and narrow light absorption edge in previous reports, it is expected that the photocatalytic performance of CQDs/Bi_2MoO_6 could be further improved by enhancing these two properties. Therefore, this study focused on exploring feasible preparation methods to synthesize CQDs/Bi_2MoO_6 with a wider range of light absorption and larger specific surface area.

In this study, an alcohol-thermal method was adopted to synthesize three-dimensional microspherical CQDs/Bi_2MoO_6 heterostructures. The chemical composition, microscopic morphology, pore structure, chemical valence, and optical properties of the synthesized CQDs/Bi_2MoO_6 were investigated. The photocatalytic degradation and mineralization performance on antibiotic norfloxacin were examined, from which the optimal loading amount of CQDs was determined. The photocatalytic mechanism was proposed accordingly. Moreover, in order to evaluate the application potential of the synthesized CQDs/Bi_2MoO_6 in real aquatic environment, optimization experiments including norfloxacin concentration, catalyst dosage, pH, and coexisting anion, were further investigated.

The three-dimensional microspherical CQDs/Bi_2MoO_6 heterostructures were synthesized using a simple alcohol-thermal method. CQDs/Bi_2MoO_6 with different CQDs loading amount were synthesized, in which CQDs were mainly added by taking the supernatant obtained from the hydrothermal method as a stock solution, and the CQDs loading was adjusted by controlling the volume of added CQDs stock solution, and the samples synthesized with the addition of 0, 100, 200, and 300 μL of the CQDs stock solution were named Bi_2MoO_6, 100-CQDs/Bi_2MoO_6, 200-CQDs/Bi_2MoO_6, and 300-CQDs/Bi_2MoO_6, respectively. Detailed materials, synthesis, characterization and photocatalytic activity measurement was shown in Supporting information. With X-ray diffraction (XRD), the phase structures of Bi_2MoO_6 and CQDs/Bi_2MoO_6 composites were measured. Fig. 1a demonstrated that the pure Bi_2MoO_6 showed obvious and sharp characteristic peaks at 2θ of 28.2°, 32.5°, 46.7°, 55.4°, and 58.5°, which coincided with the orthogonal phase Bi_2MoO_6 (JCPDS No. 21–0102) planes (131), (200), (202), (331), and (262). No other peak was observed in the Bi_2MoO_6 sample, suggesting no impurity in the synthesized Bi_2MoO_6. In the CQDs/Bi_2MoO_6 composites, all peaks of Bi_2MoO_6 were determined and showed a shift to a lower angle, which was probably due to the existence of strong interfacial interactions between the CQDs and Bi_2MoO_6 resulting in a slight distortion of the Bi_2MoO_6 lattice [21]. In addition, with the introduction of CQDs, the peaks of Bi_2MoO_6 showed slight weakening and broadening, indicating that its crystallinity deteriorated. Notably, no characteristic peak of CQDs was identified, which might be attributed to the CQDs/Bi_2MoO_6 composites' low concentration and high dispersion of CQDs [22]. The same observations were obtained from other similar systems [20].

Fig. 1b showed the Fourier transform infrared (FT-IR) spectra of different samples, from which it is clear that the absorption peaks of the Bi_2MoO_6 sample appeared at 1620, 840, 729, 557, and 441 cm^{-1}. Among the five absorption peaks, the adsorbed water molecule's H-O bending vibration was at 1620 cm^{-1}. The Mo-O bond stretching vibration induced a peak of 840 cm^{-1} [8], there was an asymmetric stretching pattern of the equatorial oxygen atoms in the MoO_6^{6-} layer resulting in a peak at 729 cm^{-1} [23], on 557 cm^{-1} the absorption peak was originated from the MoO_6^{6-} based bending vibration [24], while the 441 cm^{-1} absorption peak was responsible for stretching vibrations of Bi-O bonds in Bi_2MoO_6. In all CQDs/Bi_2MoO_6 composites, the five absorption peaks of Bi_2MoO_6 were clearly observed, as well as a new absorption peak at 1390 cm^{-1} appeared. A 1390 cm^{-1} peak was found to correlate with the C-O-C tension vibration, indicating that CQDs was present in all CQDs/Bi_2MoO_6 composites [25].

The high-resolution X-ray photoelectron spectroscopy (XPS) spectra for Bi_2MoO_6 as well as 200-CQDs/Bi_2MoO_6 were evident that both of them contained binding energy peaks for four elements: O, Mo, Bi and C (Fig. S2 in Supporting information), where C in Bi_2MoO_6 was mainly derived from contaminated carbon in the environment and instruments [26]. In Fig. 1c, the 232.4 eV and 235.5 eV signature peaks correspond to Mo $3d_{5/2}$ and Mo $3d_{3/2}$, indicating that Mo^{6+} was present in Bi_2MoO_6. The 159.2 eV and 164.5 eV characteristic peaks of Fig. 1d were induced by Bi $4f_{7/2}$ and Bi $4f_{5/2}$, demonstrating the existence of Bi as Bi^{3+} [13]. In Fig. 1e, the distinctive peaks at 530.0 eV, 530.6 eV, and 531.4 eV, respectively, were the Bi-O, Mo-O, and C = O bonds [27,28]. The separation of the C 1s peaks in Fig. 1f occurred at energies corresponding to the C-C sp^2-hybridized carbon, the C-O-C bond, and the C=O bond of CQDs, respectively, at 284.8 eV, 286.2 eV, and 288.4 eV [29], proving that the composite catalyst was effectively infused with CQDs, which was consistent with the FTIR analysis. It was observed that after the decorating with CQDs, the characteristic peak of Mo $3d_{5/2}$ shifted from 232.4 eV to 232.3 eV, whereas the Mo $3d_{3/2}$ shifted from 235.5 eV to 235.4 eV. Simultaneously, the characteristic peak of Mo-O bonds in O 1s shifted from 530.6 eV to 530.9 eV. Obviously, these shifts were attributed to the presence of CQDs, suggesting the formation of Mo-O-C bonds [26,30].

The scanning electron microscopy (SEM) image of obtained sample suggested that Bi_2MoO_6 was a three-dimensional microsphere composed of nanorods (Fig. 2a). With its rough surface, there should be plenty of active sites on the catalyst surface according to the Bi_2MoO_6's huge specific surface area [23]. The prepared CQD's image was shown using high-resolution transmission electron microscopy (HRTEM) in Fig. 2b. The 0.33 nm lattice stripe corresponded with (002) crystal plane on CQDs [19], suggesting that the hydrothermal approach had been successfully used to create CQDs. Moreover, as shown, the CQDs were made up of uniformly small particles with a diameter of around 6 nm. Fig. 2c displayed the TEM picture of the 200-CQDs/Bi_2MoO_6 composite, which can be clearly seen as a rod-like structure. From 200-CQDs/Bi_2MoO_6 HRTEM images shown as Fig. 2d, 0.23 and 0.28 nm lattice spacing respectively matched the (100) crystal plane of

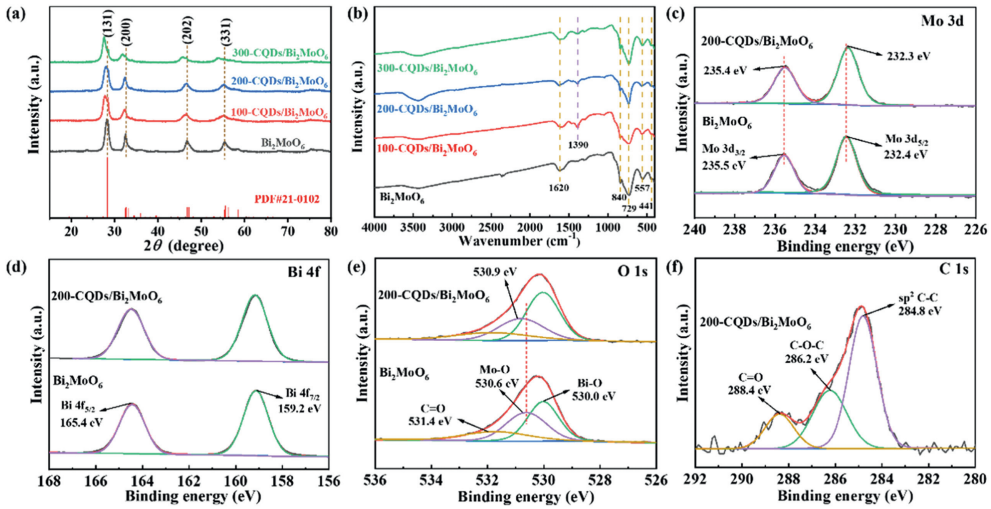

Fig. 1. Phase structure and chemical composition of the as-prepared catalysts. (a) The XRD patterns. (b) The FTIR spectra. (c) Mo 3d spectra. (d) Bi 4f spectra. (e) O 1s spectra. (f) C 1s spectra.

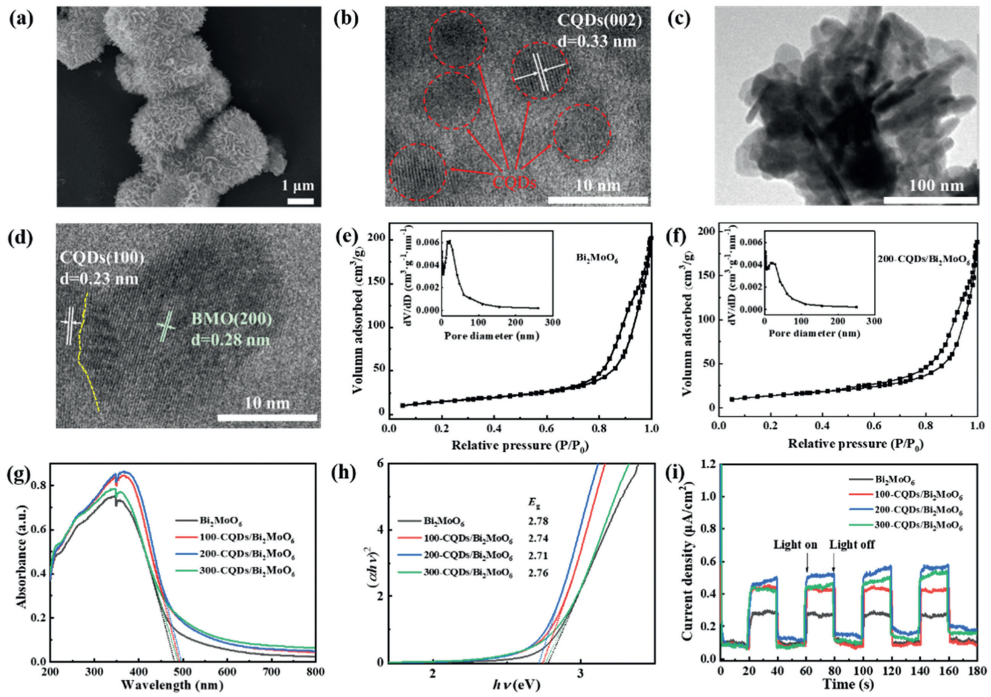

Fig. 2. Morphology, pore structure, optical absorption and electrochemical properties of the as-prepared catalysts. (a) SEM images of Bi_2MoO_6. (b) HRTEM images of CQDs. (c) TEM image of the 200-CQDs/Bi_2MoO_6. (d) HRTEM images of 200-CQDs/Bi_2MoO_6. (e, f) Nitrogen adsorption isotherm of the Bi_2MoO_6 and 200-CQDs/Bi_2MoO_6. (g) The UV–vis absorption spectra of the Bi_2MoO_6 and CQDs/Bi_2MoO_6. (h) The plots of $(\alpha h\nu)^2$ *versus* energy ($h\nu$) of the Bi_2MoO_6 and CQDs/Bi_2MoO_6. (i) The transient photocurrent response of Bi_2MoO_6 and 200-CQDs/Bi_2MoO_6.

CQDs [31] and that of Bi_2MoO_6 (200) crystal plane. The obvious interface between the lattice of CQDs and Bi_2MoO_6 demonstrated that the synthesized CQDs/Bi_2MoO_6 is a heterojunction structure, where the heterojunction structure was reported to be able to facilitate electron-hole pairs separation and lengthen photogenerated electron and hole lifetimes [19].

Figs. 2e and f illustrated the information about the pore size and nitrogen (N_2) adsorption isotherms on the prepared Bi_2MoO_6 and 200-CQDs/Bi_2MoO_6. The nitrogen adsorption-desorption isotherms of both Bi_2MoO_6 and 200-CQDs/Bi_2MoO_6 corresponded to type IV of the BDDT (Brunauer-Deming-Deming-Teller) classification, which suggested that Bi_2MoO_6 and 200-CQDs/Bi_2MoO_6 were mesoporous materials [32]. The specific surface area (SSA) of the catalysts was mainly calculated based on the Brunauer-Emmett-Teller (BET) test method and the results were displayed in Table 1. The SSA of Bi_2MoO_6, 100-CQDs/Bi_2MoO_6, 200-CQDs/Bi_2MoO_6, and 300-CQDs/Bi_2MoO_6 were 54.4, 54.9, 56.0 and 57.6 m^2/g respectively, which are at a relatively high level compared to the existing reports (Table S1 in Supporting information). From this, the introduction of CQDs could slightly increase the specific surface area of the catalyst, which could facil-

Table 1
The specific surface area of the Bi_2MoO_6 and CQDs/Bi_2MoO_6 composites.

Catalysts	Bi_2MoO_6	100-CQDs/Bi_2MoO_6	200-CQDs/Bi_2MoO_6	300-CQDs/Bi_2MoO_6
SSA (m^2/g)	54.4	54.9	56.0	57.6

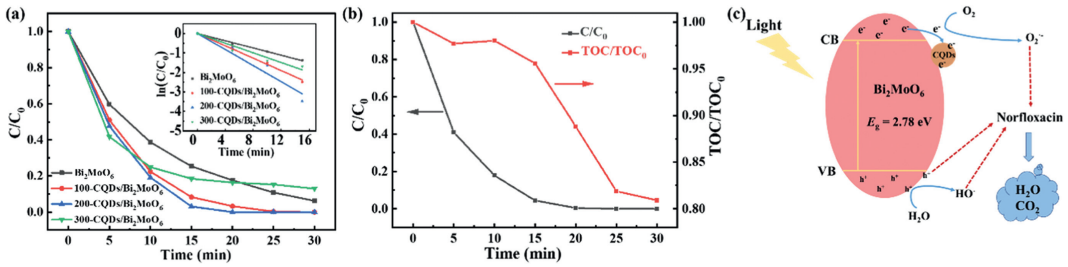

Fig. 3. (a) Degradation of norfloxacin on Bi_2MoO_6 and CQDs/Bi_2MoO_6. (b) The photocatalytic degradation and TOC removal curves of norfloxacin on 200-CQDs/Bi_2MoO_6 catalyst. (c) The possible photocatalytic mechanism for norfloxacin degradation over CQDs/Bi_2MoO_6 catalyst ([norfloxacin] = 20 mg/L, [catalysts] = 0.8 g/L, pH 7).

itate the contact between the contaminants and the catalyst [18]. However, the different loading amount of CQDs showed similar effects on the specific surface area. This observation is the agreement with the previous literature, where in Di's study [19], the SSA of the CQDs/Bi_2MoO_6 composite slightly increased from 6.08 m^2/g to 8.68 m^2/g after loading CQDs. In Sun's study [20], with the increment in loading of CQDs reagent to 0.1 g from 0.05 g, the SSA rose to 16.83 m^2/g from 16.27 m^2/g. It is worth noting that our prepared CQDs/Bi_2MoO_6 composite showed a much bigger SSA, which ascribed to our preparation method is beneficial to produce CQDs/Bi_2MoO_6 with high specific surface area. The larger the SSA, the more active sites available in the photocatalytic process and better the degradation performance [22].

The UV–vis diffuse reflectance spectra (DRS) from Bi_2MoO_6 and CQDs/Bi_2MoO_6 composites were displayed in Fig. 2g. It can be seen that each sample exhibited absorption edges at 480–496 nm, indicating that an excellent visible light absorption ability of the synthesized catalysts. Compared with pure Bi_2MoO_6, as mentioned in the introduction the loading of CQDs could significantly enhance the visible light absorption intensity of CQDs/Bi_2MoO_6, in addition, our synthesized CQDs/Bi_2MoO_6 also exhibited broadened absorption edges, among which 200-CQDs/Bi_2MoO_6 exhibited the largest absorption edge (broadening the absorption edge of the pure Bi_2MoO_6 from 480 nm to 496 nm) and the strongest visible light absorption intensity. Fig. 2h displayed for the prepared sample the band gap. It was evident that Bi_2MoO_6 had a band gap of 2.78 eV. Band gaps of CQDs/Bi_2MoO_6 composites were tuned with the CQDs content, among which 200-CQDs/Bi_2MoO_6 owned the lowest band gap of 2.71 eV. From above, it is evident that adding CQDs to Bi_2MoO_6 considerably increased the catalyst's visible light usage, in which 200-CQDs/Bi_2MoO_6 showed the optimal visible light absorption performance [24]. This broader absorption edge and lower band gap may be attributed to the role of CQDs, it functioned by enhancing the intensity of visible light absorption [22], which would absorb more visible light thus causing CQDs/Bi_2MoO_6 to exhibit enhanced visible light absorption. Besides, the upconversion feature of CQDs may be responsible for the absorption edge's expansion [33], where the CQDs could emit light at shorter wavelengths of 300–530 nm when they were excited with light at 700–1000 nm [34]. So as the loading amount of CQDs increased from 0 μL to 200 μL, the bandgap of CQDs/Bi_2MoO_6 gradually lowered. While continuing to increase the loading of CQDs to 300 μL, the bandgap of 300-CQDs/Bi_2MoO_6 became higher instead, which might be due to the overloading of 300 μL CQDs resulting in the accumulation of CQDs on the surface of Bi_2MoO_6, it would hinder light absorption of Bi_2MoO_6 and produced an internal filtering effect on light [35], which resulted in the poorer light absorption performance.

The transient photocurrent response curves of Bi_2MoO_6 and CQDs/Bi_2MoO_6 were tested to study charge separation (Fig. 2i). The CQDs/Bi_2MoO_6 composite showed a larger photocurrent intensity than the pure Bi_2MoO_6, indicating its better electron-hole separation efficiency and longer electron lifetime. The increase in photocurrent intensity may be related to CQDs' ability to transport electrons, which served as an electron collector, capturing electrons spawned from the Bi_2MoO_6 semiconductor to prolong the carrier lifetime [36]. And the photocurrent intensity increased with the increase of CQDs loading amount from 100 μL to 200 μL, further increasing the CQDs loading amount to 300 μL, the photocurrent intensity decreased instead.

The degradation of norfloxacin by Bi_2MoO_6 and CQDs/Bi_2MoO_6 composites was tested under visible light in Fig. 3a. It showed that the photodegradation rate of 200-CQDs/Bi_2MoO_6 reached 99% within 30 min, which were notably greater than Bi_2MoO_6, 100-CQDs/Bi_2MoO_6, and 300-CQDs/Bi_2MoO_6. As shown in Table S2 (Supporting information), the CQDs/Bi_2MoO_6 photocatalyst synthesized in this study exhibited obviously superior performance compared to the reported photocatalysts for the degradation of norfloxacin by visible light irradiation. The inset in Fig. 3a showed the results of the fitting using the *quasi*-first order kinetic model, in which k (where the absolute value of the slope of the line represented the k value) presented at first an increasing tendency followed by a decreasing tendency with an increase in CQDs amount, where the 200-CQDs/Bi_2MoO_6 composite exhibited a maximum reaction rate constant as 0.2066 min^{-1}. Combined with the photocurrent test results, it is speculated that it may be due to the addition of CQDs, where the CQDs acted as the electron trapping agent and the construction of the CQDs/Bi_2MoO_6 heterojunction benefited the transferring of electrons from Bi_2MoO_6 to CQDs, which improved the efficiency of photogenerated electron-hole separation to prolong electron as well as hole longevity in order to degrade pollutants [29]. Meanwhile, combined with the DRS results, it could be known that the presence of CQDs broadened the spectral response range of the catalyst. Moreover, the upconversion luminescence property of CQDs resulted in its ability to emit shorter wavelengths of light in stimulation of the photocatalyst after absorbing near-infrared light [34], thereby enhancing the photocatalytic behavior. The performance was considerably impacted by the CQDs loading amount, namely, CQDs/Bi_2MoO_6 composites demonstrated an increment in photocatalytic activity in response to the growth of CQDs loading, where 200-CQDs/Bi_2MoO_6 reached the best performance. This is mainly because 200-CQDs/Bi_2MoO_6 exhibited the largest absorption edge (broadening the absorption edge of the pure Bi_2MoO_6 from 480 nm to 496 nm), the strongest visible light absorption intensity and the best electron-hole separation efficiency.

For further evaluation of mineralization ability of the 200-CQDs/Bi_2MoO_6 photocatalyst, the change of TOC was monitored during the norfloxacin degradation. The TOC removal rate was approximately 20% in 30 min, as illustrated in Fig. 3b. This result indicated that the CQDs/Bi_2MoO_6 photocatalyst can effectively mineralize norfloxacin to CO_2 when exposed to visible light [6]. It merits our attention that the norfloxacin decay was fast in the first 15 min when the TOC removal was almost inert. This observation should be ascribed to the photocatalytic reaction in the earlier stage mainly degraded the norfloxacin to small organic molecules

rather than CO_2. Prolonging the reaction time to 30 min, the norfloxacin decay leveled off since the norfloxacin almost completely degraded while the TOC removal was accelerated, which might be because the small organic molecules started to convert into CO_2 right after the destruction of the target norfloxacin molecules. Therefore, it can be deduced that if the experimental time is extended, the TOC can still maintain a certain rate of removal [37].

In light of aforementioned findings, Fig. 3c presented mechanisms for norfloxacin's degradation under this system. When the CQDs/Bi_2MoO_6 photocatalyst was illuminated by light, the catalyst generated hole-electron (h^+ and e^-) pairs under the stimulation of light, and then the excited electrons skipped to the conduction band (CB) from the valence band (VB) to generate holes (h^+_{VB}) and electrons (e^-_{CB}). The CQDs acting as electron carriers could trap the photogenerated e^-, thus effectively preventing the combination of h^+ and e^-. As known in the reported literature, the E_{VB} of Bi_2MoO_6 was +2.34 eV [38], which was more positive than that of $H_2O/HO^•$ (+2.27 eV *vs.* NHE) [39], so the h^+ produced in Bi_2MoO_6 could oxidize H_2O to $HO^•$, and the E_{CB} of Bi_2MoO_6 was −0.34 eV, which was more negative than that of $O_2/O_2^{•-}$ (−0.28 eV *vs.* NHE), so the e^+ generated in Bi_2MoO_6 could reduce O_2 to $O_2^{•-}$ [18,40,41]. In the CQDs/Bi_2MoO_6 system, the norfloxacin can be degraded by the h^+_{Vb}, $HO^•$ and $O_2^{•-}$. The detailed reaction mechanism is shown in Eqs. (1)-(4).

$$CQDs/Bi_2MoO_6 + h\nu \rightarrow h^+_{VB} + e^-_{CB} \quad (1)$$

$$e^-_{CB} + O_2 \rightarrow O_2^{•-} \quad (2)$$

$$h^+_{VB} + H_2O \rightarrow HO^• + H^+ \quad (3)$$

$$\left(O_2^{•-},\ HO^•,\ h^+_{VB}\right) + \text{norfloxacin} \rightarrow \text{products} \quad (4)$$

The impact of operating factors, such as the catalyst dose, norfloxacin's starting concentration, as well as pH level, on the degradation of norfloxacin was depicted in Fig. S3 (Supporting information). Figs. S3a and b displayed the effect of different dosages of catalyst on the degradation of norfloxacin. In Fig. S3a, the degradation of norfloxacin by light alone was also investigated, *i.e.*, at the catalyst dosage of 0 g/L, it was clear from the figure that there was almost no degradation of norfloxacin by light alone. And there was a continuous rise in k up to 0.2066 min^{-1} from 0.0749 min^{-1} if the dosage of CQD/Bi_2MoO_6 was raised to 0.8 g/L from 0.3 g/L and then a decrease as the dosage of CQD/Bi_2MoO_6 increased unceasingly. The creation of a significant amount of photo-generated h^+ and e^- from the higher catalyst dosage contributed to the rise in k, which in turn generated abundant radicals to degrade norfloxacin [13]. Nevertheless, once CQDs/Bi_2MoO_6 was dosed at concentrations exceeding 0.8 g/L, the catalyst should gradually weaken the light transmission of the solution and produce a physical masking effect [42], causing the catalyst to absorb less light and generate fewer radicals. Furthermore, if the catalyst overdosed, the excess radicals would self-react with deactivation, as described in Eq. 5 [43]. Therefore, the best amount of catalyst to use was considered as 0.8 g/L in this study by considering the degradation rate of norfloxacin.

$$HO^• + HO^• \rightarrow H_2O_2 \quad (5)$$

It was investigated how norfloxacin's initial concentrations affected the rate of degradation. Figs. S3c and d displayed that there was a drop in norfloxacin degradation efficiency in response to an increment in the norfloxacin concentration, *i.e.*, there was a continuous decrease in k to 0.0934 min^{-1} from 0.3019 min^{-1} if norfloxacin initial concentration was raised to 25 mg/L from 10 mg/L. It is presumed that the active site's utilization of the catalyst reached saturation at higher norfloxacin concentrations, and the same amount of catalyst cannot degrade more norfloxacin at a certain time; in other words, the greater initial norfloxacin concentration solution was deficient in reactive free radicals [13].

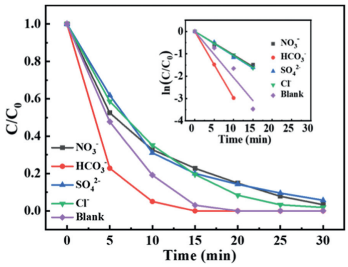

Fig. 4. Effect of coexisting ions on norfloxacin degradation.

In addition, higher concentrations of norfloxacin absorbed more photons, leaving relatively fewer photons available for the active catalyst, and the shortage of photons on the catalyst surface somewhat delayed the initial stage in the photocatalytic reaction, namely the activation to catalyst by absorbing photons, thus decreasing the degradation rate of norfloxacin [35]. Besides, there were more intermediates generated in the degradation at higher norfloxacin concentrations, which would compete with norfloxacin for the active radicals, rendering the degradation rate of norfloxacin declined [44].

Photocatalytic degradation tests were performed in solutions with different pH values for the purpose of understanding how the pH affected the degradation of norfloxacin. Figs. S3e and f revealed that norfloxacin degradation was inhibited in the strong acid (pH 2.2) and strong base (pH 12.0), and the degradation efficiency of norfloxacin was only 11.48% and 70.22% after 30 min of reaction, respectively, with k values of 0.0064 min^{-1} and 0.0918 min^{-1}. This is mainly related to the interaction of the catalyst's surface charge with the contaminant. Bi_2MoO_6 is purported to have a zero point charge of 6.1 [45,46], therefore, as pH < 6.1, there are positive charges on the catalyst surface, and as pH > 6.1, there are negative charges. The carboxyl and piperazine groups, which have pK_a values of 6.2 and 8.5, respectively, are the norfloxacin's two proton-binding sites. When the pH is lower than 6.2, there are positive charges of the norfloxacin molecule. With pH values ranging from 6.2 to 8.5, the norfloxacin molecule is electrically neutral and has both positive and negative charges; and when the pH is greater than 8.5, the norfloxacin molecule is negatively charged [47]. The catalyst's surface was strongly positively and negatively charged when pH 2.2 or 12.0, respectively, which strongly repulse the same charged norfloxacin, weakening the binding affinity between the norfloxacin and CQDs/Bi_2MoO_6 composite and thus inhibiting the norfloxacin decay. In contrast, norfloxacin breakdown was favored by an intermediate pH scope (pH 4.4 to 10.8), with the pH adjusted from 4.4 to 10.8, the degradation efficiency all exceeded 94% in 30 min. In detail, the k increased with increasing pH between pH 4.4 and 10.8, and the optimum pH level was determined at pH 10.8 with the biggest k of 0.5278 min^{-1}. That is because a higher pH level provided more hydroxyl ions, which resulted in more hydroxyl radicals during the photocatalytic process and efficient norfloxacin decay. As a result, the photocatalyst CQDs/Bi_2MoO_6 operated well at a wide pH range, which is a great advantage in practice.

It was necessary by analyzing CQDs/Bi_2MoO_6 degradation properties within an interfering substance presence to simulate its application potential in real water. Separate experiments on norfloxacin degradation in the presence of HCO_3^-, Cl^-, NO_3^-, and SO_4^{2-} were conducted. Fig. 4 demonstrated that HCO_3^- aided norfloxacin decomposition, whereas other anions such as Cl^-, NO_3^-, and SO_4^{2-} inhibited norfloxacin degradation at a certain degree.

With the addition of HCO_3^-, degradation performance enhanced as the k having gone up to 0.2974 min^{-1} from 0.2066 min^{-1}. It is assumed that the $CO_3^{\bullet-}$ could be generated by the reaction between HCO_3^- and $HO^\bullet$ through Eq. 6. Despite the formed $CO_3^{\bullet-}$ being less active than $HO^\bullet$ [48], $CO_3^{\bullet-}$ is reported to be a more selective active species than $HO^\bullet$, which can rapidly react with the substances containing the aromatic aniline functional group [49]. Considering the target norfloxacin is one of the substances containing aromatic aniline, therefore, it can be easily oxidized and degraded in the presence of $CO_3^{\bullet-}$ [7]. Moreover, it was monitored that the addition of HCO_3^- made the solution alkaline, with a pH around 8.4. The effect of pH on the system from the previous section indicates that the reaction is more suitable for weakly alkaline conditions, which is also one of the reasons why the presence of HCO_3^- exhibited a facilitative effect on norfloxacin photocatalytic degradation.

$$HO^\bullet + HCO_3^- \rightarrow H_2O + CO_3^\bullet \quad (6)$$

The addition of Cl^-, NO_3^-, and SO_4^{2-} all inhibited norfloxacin degradation to some extent. It is mainly because Cl^-, NO_3^-, and SO_4^{2-} can all act as scavengers of $HO^\bullet$, through the Eqs. 7-9, giving rise to less active species such as $ClHO^{\bullet-}$, $NO_3^\bullet$, and $NO_2^\bullet$ [13,48,50]. Because freshly created radicals had a lower oxidizing capacity than consumed $HO^\bullet$, decomposition of norfloxacin had been suppressed when Cl^-, NO_3^-, and SO_4^{2-} existed.

$$Cl^- + HO^\bullet \rightarrow ClHO^{\bullet-} \quad (7)$$

$$NO_3^- + HO^\bullet \rightarrow OH^- + NO_3^\bullet \quad (8)$$

$$NO_3^\bullet + H_2O + e^- \rightarrow 2OH^- + NO_2^\bullet \quad (9)$$

In this study, three-dimensional microspheres of $CQDs/Bi_2MoO_6$ in heterojunction structure were synthesized by an alcohol-thermal method. The 200-$CQDs/Bi_2MoO_6$ showed the best performance among the catalysts with different CQDs amounts, which showed a large specific surface area of 56.0 m^2/g and the extending light-absorption edge from 480 nm to 496 nm. The intimate contact between Bi_2MoO_6 and CQDs resulted in the formation of Mo-O-C bonds and the improved interfacial charge transfer. The optimal degradation effect of 20 mg/L norfloxacin was obtained when the catalyst dosage = 0.8 g/L and pH 4.4–10.8, *i.e.*, 99% norfloxacin degradation efficiency and 20% TOC removal were achieved in 30 min. Moreover, the coexistence of anions such as HCO_3^-, Cl^-, NO_3^-, and SO_4^{2-} did not significantly impact the photocatalytic performance. In summary, the $CQDs/Bi_2MoO_6$ composite is an effective photocatalyst for the removal and mineralization of norfloxacin in real aqueous environments.

Declaration of competing interest

The authors declare that they have no known competing financial interests or personal relationships that could have appeared to influence the work reported in this paper.

Acknowledgments

This work was funded by the National Science Foundation of China (Nos. 42377452 and 41877481), the Strategic Priority Research Program of the Chinese Academy of Sciences, China (Nos. XDA23010300 and XDA23010000), the Opening Fund of Key Laboratory of Aerosol Chemistry and Physics, Institute of Earth Environment, CAS (No. KLACP2002). Thanks to Miss Chenyu Liang from the Instrumental Analysis Center and Ms. Xiaojing Zhang from School of Physics at Xi'an Jiaotong University for their assistance.

Supplementary materials

Supplementary material associated with this article can be found, in the online version, at doi:10.1016/j.cclet.2023.109336.

References

[1] M.S. de Ilurdoz, J.J. Sadhwani, J.V. Reboso, J. Water Process. Eng. 45 (2022) 102474.
[2] L. Catteau, L. Zhu, F. Van Bambeke, et al., Phytochem. Rev. 17 (2018) 1129–1163.
[3] A. Jia, Y. Wan, Y. Xiao, et al., Water Res. 46 (2012) 387–394.
[4] W. Deng, N. Li, H. Zheng, et al., Ecotoxicol. Environ. Saf. 125 (2016) 121–127.
[5] M. Chen, Y. Huang, W. Chu, Chin. J. Catal. 40 (2019) 673–680.
[6] W. Wang, Z. Zeng, G. Zeng, et al., Chem. Eng. J. 378 (2019) 122132.
[7] F. Zhu, Y. Wu, Y. Liang, et al., Chem. Eng. J. 389 (2020) 124276.
[8] T. Chankhanittha, V. Somaudon, J. Watcharakitti, et al., J. Mater. Sci.: Mater. Electron. 32 (2021) 1977–1991.
[9] H. Yi, C. Lai, X. Huo, et al., Environ. Sci.: Nano 9 (2022) 815–826.
[10] J.S. Wang, X.H. Yi, X. Xu, et al., Chem. Eng. J. 431 (2022) 133213.
[11] H. Mohtasham, M. Rostami, B. Gholipour, et al., Chemosphere 310 (2023) 136625.
[12] P. Dhiman, G. Rana, R.A. Alshgari, et al., Environ. Res. 216 (2023) 114665.
[13] Z. Shen, H. Zhou, Z. Pan, et al., J. Hazard. Mater. 400 (2020) 123187.
[14] H. Ma, Y. He, X. Li, et al., Appl. Catal. B 292 (2021) 120159.
[15] S. Li, S. Hu, W. Jiang, et al., J. Colloid Interface Sci. 556 (2019) 335–344.
[16] G. Zhang, D. Chen, N. Li, et al., Appl. Catal. B 250 (2019) 313–324.
[17] Q. Zhao, Z. Zhang, T. Yan, et al., RSC Adv. 11 (2021) 28674–28684.
[18] Z. Zhang, T. Zheng, J. Xu, et al., J. Photochem. Photobiol. A 346 (2017) 24–31.
[19] J. Di, J. Xia, M. Ji, et al., Nanoscale 7 (2015) 11433–11443.
[20] C. Sun, Q. Xu, Y. Xie, et al., J. Alloys Compd. 723 (2017) 333–344.
[21] X. Miao, Z. Ji, J. Wu, et al., J. Colloid Interface Sci. 502 (2017) 24–32.
[22] J. Wang, L. Tang, G. Zeng, et al., Appl. Catal. B 222 (2018) 115–123.
[23] A. Phuruangrat, S. Buapoon, T. Bunluesak, et al., J. Aust. Ceram. Soc. 58 (2022) 999–1008.
[24] X. Lü, J. Shen, D. Fan, et al., Res. Chem. Intermed. 41 (2015) 9629–9642.
[25] J. Wang, F. Han, Y. Rao, et al., Ind. Eng. Chem. Res. 57 (2018) 10226–10233.
[26] J. Zhao, Y. Yang, W. Yu, et al., J. Mater. Sci. Mater. Electron. 28 (2017) 543–552.
[27] L. Zhang, Z. Wang, C. Hu, et al., Appl. Catal. B 257 (2019) 117785.
[28] T. Zhou, J. Hu, J. Li, Appl. Catal. B 110 (2011) 221–230.
[29] X. Sun, W. He, T. Yang, et al., Chem. Eng. J. 412 (2021) 128679.
[30] W. Dai, W. Xiong, J. Yu, et al., ACS Appl. Mater. Interfaces 12 (2020) 25861–25874.
[31] Y. Zhang, L. Wang, X. Ma, et al., J. Colloid Interface Sci. 531 (2018) 47–55.
[32] R. Abazari, A.R. Mahjoub, J. Shariati, et al., J. Cleaner Prod. 221 (2019) 582–586.
[33] H. Zhang, H. Huang, H. Ming, et al., J. Mater. Chem. 22 (2012) 10501–10506.
[34] Y. Su, M. Xie, X. Lu, et al., RSC Adv. 4 (2014) 4839–4842.
[35] C. Guo, J. Xu, S. Wang, et al., Catal. Sci. Technol. 3 (2013) 1603–1611.
[36] M. Ji, Z. Zhang, J. Xia, et al., Chin. Chem. Lett. 29 (2018) 805–810.
[37] S. Li, S. Hu, W. Jiang, et al., J. Colloid Interface Sci. 530 (2018) 171–178.
[38] X. Gao, W. Du, X. Gong, et al., Opt. Mater. 105 (2020) 109828.
[39] P. Peng, Z. Chen, X. Li, et al., Sep. Purif. Technol. 291 (2022) 120901.
[40] X. Gao, X. Ji, T.T. Nguyen, et al., Vacuum 164 (2019) 256–264.
[41] Y. Qu, X. Li, H. Zhang, et al., J. Hazard. Mater. 429 (2022) 128310.
[42] Z. Chen, X. Li, Q. Xu, et al., Chem. Eng. J. 390 (2020) 124454.
[43] Y. Liu, X. He, Y. Fu, et al., Chem. Eng. J. 284 (2016) 1317–1327.
[44] Y. Wang, D. Tian, W. Chu, et al., Sep. Purif. Technol. 212 (2019) 536–544.
[45] M. Long, W. Cai, H. Kisch, Chem. Phys. Lett. 461 (2008) 102–105.
[46] J. Zhang, T. Wang, X. Chang, et al., Chem. Sci. 7 (2016) 6381–6386.
[47] W. Yang, Y. Lu, F. Zheng, et al., Chem. Eng. J. 179 (2012) 112–118.
[48] J. Li, M. Xu, G. Yao, et al., Chem. Eng. J. 348 (2018) 1012–1024.
[49] X.H. Wang, A.Y.C. Lin, Environ. Sci. Technol. 46 (2012) 12417–12426.
[50] X. Gao, J. Niu, Y. Wang, et al., J. Hazard. Mater. 403 (2021) 123860.